IET Electric Power Applications

Research Article

Modified predictive torque and flux control for open end winding induction motor drive based on ranking method

ISSN 1751-8660
Received on 15th October 2017
Revised 7th December 2017
Accepted on 18th December 2017
E-First on 18th January 2018
doi: 10.1049/iet-epa.2017.0679
www.ietdl.org

Kodumur Meesala Ravi Eswar[1] ✉, Kunisetti V. Praveen Kumar[1], Thippiripati Vinay Kumar[1]
[1]Department of Electrical Engineering, National Institute of Technology, Warangal, India
✉ *E-mail: nit.ravieswar@gmail.com*

Abstract: The emerging application of predictive torque and flux control (PTC) in induction motor (IM) drive technology is becoming more successful. The PTC scheme can be applied to open-end winding IM (OEWIM) drive fed by dual inverter owing to its merits: high dynamic performance, simple control by involving regulation parameters into the control law. However, a conventional PTC offers single control law. To achieve controlling of multiple parameters, weighting factors need to be assigned to the respective parameters in the control law. The selection of weighting factors directly affects control performance of OEWIM. For an optimal selection of weighting factors, the empirical method has to be followed, which is time overwhelming and cumbersome process. To overcome this problem, this study introduces multi-objective controlling and optimisation based on the ranking method rather than the minimisation of single control law as in the case of conventional methods. The proposed feature circumvents optimisation of weighting factors. To validate the proposed scheme, simulation using Matlab/Simulink and experimental analysis are performed for dual-inverter fed OEWIM drive. By considering same control objectives (torque, flux ripple and switching frequency limitation), these results are examined with a conventional PTC scheme to accentuate merits of the proposed scheme.

1 Introduction

Variable speed induction motor (IM) drives fed by voltage source inverters (VSIs) became more popular for industrial applications. The current development is to use multilevel inverters (MLIs) for electric drive applications [1]. The increase in the number of voltage vectors means precise control, improvement of torque and flux regulation [1]. Apart from MLIs present in [2–4], the multilevel inversion with dual-inverter fed open-end winding IM (OEWIM) drive attains prominent status owing to its merits: simple structure, elimination of clamping diodes as related to the neutral point clamped (NPC) structure, requirement of fewer DC-link voltages compared to cascaded H-bridge inverter configuration. The several applications of OEWIM drive are documented in [5]. To improve the dynamic response of the drive, several control methods are introduced. The first innovation is started with field oriented control of IM drive in former 1960s [6–8]. The controlling is achieved in a rotating frame of reference. Requirement of current proportional–integral (PI) regulators, rotor flux observer and reference frame transformations hike computational complexity of the control scheme. To overcome these demerits, direct torque control (DTC) is hosted in the year 1986 [9]. It offers controlling in a stationary frame of reference and has a direct impact on torque control by applying appropriate voltage vector. The limitations of this scheme are the following: The inclusion of non-linear hysteresis controllers (flux and torque) demands high sampling frequency in a digital platform, large ripples in torque and flux, dependent of switching frequency on hysteresis band and motor speed. These limitations are addressed in [10–14].

Recently predictive control is introduced in control process [15]. It is applicable for both converter and electric drive applications [16–19]. Model predictive control (MPC) is the part of the predictive control and it is classified into two types. They are continuous control set MPC and finite control set MPC (FCS-PTC). FCS-PTC is gaining more importance and emerging technology in the field of electric drives. Its intuitive nature, simple control, direct involvement of control parameters, the absence of heuristic look-up tables and hysteresis controllers highlighted the advantages of PTC over the existing control schemes. In [20, 21], PTC for the electric drive system is performed with an extended prediction horizon. In [22], PTC is performed on IM drive fed by three-phase four-switch inverter configuration. In [23], PTC is implemented on five-leg AC–DC–AC converter powered IM drive.

In predictive control, selection of optimal switching states for an inverter is based on depreciation of control law. Control law may involve different parameters (torque, flux, common mode voltage, switching frequency and reactive power) which have to be controlled [24–26]. The involvement of different control parameters in one control law necessitates the assignment of weighting factors to the respective terms. The weighting factor assignment creates relative balance among the various control terms and plays a key role in optimal control performance. Hence, its assignment in the control law became a major issue. With the involvement of additional control terms in control law, a number of weighting factors increases and its proper tuning becomes more complex.

In [26], empirical guidelines are indicated by Cortes *et al.*, to solve the weighting factor selection problem. However, it is not an optimal selection. It is only weighting factor approximation. Determining the weights empirically, the predictive control of IM is performed in [27–33]. The analytical method is exercised in [34] to accomplish an optimal weighting factor for a three-phase VSI fed IM. It is analysed with only torque and flux control objectives. Furthermore, it involves complex control and system parameter dependent. To achieve weights optimisation in [35], multi-objective genetic algorithm (GA)-based method is adopted. It necessitates a lot of search process prior to control. For IM drive control in [36, 37], multi-decision criteria-based VIKOR and TOPSIS methods are introduced. In this process, weighting factor coefficients are not altogether removed and analysed with only torque and flux control terms. In [38], fuzzy-based online tuning of weighting factors is implemented for four-leg VSI fed IM. In [39, 40] PTC scheme is performed on OEWIM drive. Here weighting factors are selected empirically in the cost function. The tuning of the weighting factors becomes effortful and time consuming with the increase of a number of objectives. In [41], PTC is performed on the indirect matrix converter fed IM where torque ripple reduction is achieved by weighting factor optimisation.

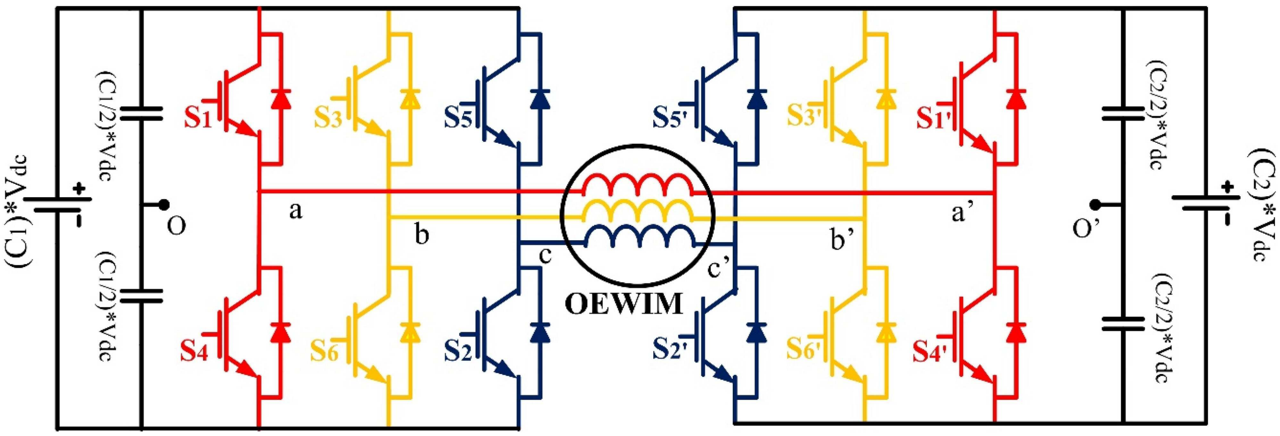

Fig. 1 *OEWIM power circuit*

This paper presents a modified FCS-PTC, where single control law is replaced by multiple objectives. The optimisation of these multiple objectives is done by ranking analysis. This simple feature enables omission of weighting factors in PTC. The proposed scheme is applied for OEWIM drive by considering three main objective functions (torque, flux control and switching frequency minimisation). The remaining part of the paper is organised as follows: Section 2 depicts the configuration of OEWIM and its mathematical modelling. Detailed information about basic PTC is explained in Section 3. Section 4 introduces the new FCS-PTC scheme. Simulation and experimental results of the proposed PTC in comparison with conventional PTC are presented in Section 5. Finally, the conclusion is derived in Section 6.

2 OEWIM configuration and mathematical modelling

Fig. 1 represents the power circuit of dual-inverter fed OEWIM. In order to achieve multi-level inversion, DC-link voltages of the dual inverter (VSI-1 and VSI-2) should be in the ratio of 2:1. Therefore, DC-link voltage of VSI-1 is maintained to $2V_{\rm dc}/3$ and for VSI-2 it is maintained to $V_{\rm dc}/3$. VSI-1 and VSI-2 pole voltages are represented by (1) and (2). From these, phase voltages are represented as (6). These phase voltages are applied to IM phases as shown in Fig. 1

$$\begin{pmatrix} V_{ao} \\ V_{bo} \\ V_{co} \end{pmatrix} = (C_1 V_{\rm dc}) \times \begin{pmatrix} S_a \\ S_b \\ S_c \end{pmatrix} \tag{1}$$

$$\begin{pmatrix} V_{a'o'} \\ V_{b'o'} \\ V_{c'o'} \end{pmatrix} = (C_2 V_{\rm dc}) \times \begin{pmatrix} S_{a'} \\ S_{b'} \\ S_{c'} \end{pmatrix} \tag{2}$$

where C_1 and C_2 are constants which are given as

$$C_1 = \frac{2}{3}, \quad C_2 = \frac{1}{3}$$

$$\begin{pmatrix} \Delta V_{aa'} \\ \Delta V_{bb'} \\ \Delta V_{cc'} \end{pmatrix} = \begin{pmatrix} V_{ao} - V_{a'o'} \\ V_{bo} - V_{b'o'} \\ V_{co} - V_{c'o'} \end{pmatrix} \tag{3}$$

The sum of pole voltage differences ($\Delta V_{aa'}$, $\Delta V_{bb'}$ and $\Delta V_{cc'}$) is not equal to zero. This indicates the presence of zero sequence voltage [5] which is given as

$$V_z = \frac{1}{3} \times (\Delta V_{aa'} + \Delta V_{bb'} + \Delta V_{cc'}) \tag{4}$$

The phase voltages are given as

$$\begin{pmatrix} V_{aa'} \\ V_{bb'} \\ V_{cc'} \end{pmatrix} = \begin{pmatrix} \Delta V_{aa'} \\ \Delta V_{bb'} \\ \Delta V_{cc'} \end{pmatrix} - \begin{pmatrix} V_Z \\ V_Z \\ V_Z \end{pmatrix} \tag{5}$$

By substitution of (4) into (5), the phase voltages are obtained in terms of pole voltages as

$$\begin{pmatrix} V_{aa'} \\ V_{bb'} \\ V_{cc'} \end{pmatrix} = \frac{1}{3} \begin{pmatrix} 2 & -1 & -1 \\ -1 & 2 & -1 \\ -1 & -1 & 2 \end{pmatrix} \times \begin{pmatrix} \Delta V_{aa'} \\ \Delta V_{bb'} \\ \Delta V_{cc'} \end{pmatrix} \tag{6}$$

The OEWIM is modelled in stationary reference frame [42]. The machine stator and rotor voltages are represented as (7) and (8). Stator and rotor flux linkages are given as (9) and (10). Electromechanical conversion is represented by (11) and (12)

$$\begin{pmatrix} V_{\rm s\alpha} \\ V_{\rm s\beta} \end{pmatrix} = R_{\rm s} \begin{pmatrix} i_{\rm s\alpha} \\ i_{\rm s\beta} \end{pmatrix} + p \begin{pmatrix} \lambda_{\rm s\alpha} \\ \lambda_{\rm s\beta} \end{pmatrix} \tag{7}$$

$$\begin{pmatrix} 0 \\ 0 \end{pmatrix} = R_{\rm r} \begin{pmatrix} i_{\rm r\alpha} \\ i_{\rm r\beta} \end{pmatrix} + p \begin{pmatrix} \lambda_{\rm r\alpha} \\ \lambda_{\rm r\beta} \end{pmatrix} + \omega_{\rm r} \begin{pmatrix} \lambda_{\rm r\beta} \\ -\lambda_{\rm r\alpha} \end{pmatrix} \tag{8}$$

$$\begin{pmatrix} \lambda_{\rm s\alpha} \\ \lambda_{\rm s\beta} \end{pmatrix} = L_{\rm s} \begin{pmatrix} i_{\rm s\alpha} \\ i_{\rm s\beta} \end{pmatrix} + L_{\rm m} \begin{pmatrix} i_{\rm r\alpha} \\ i_{\rm r\beta} \end{pmatrix} \tag{9}$$

$$\begin{pmatrix} \lambda_{\rm r\alpha} \\ \lambda_{\rm r\beta} \end{pmatrix} = L_{\rm r} \begin{pmatrix} i_{\rm r\alpha} \\ i_{\rm r\beta} \end{pmatrix} + L_{\rm m} \begin{pmatrix} i_{\rm s\alpha} \\ i_{\rm s\beta} \end{pmatrix} \tag{10}$$

$$T_{\rm motor} = \left(\frac{3}{2}\right)\left(\frac{P}{2}\right)(\lambda_{\rm s\alpha} i_{\rm s\beta} - \lambda_{\rm s\beta} i_{\rm s\alpha}) \tag{11}$$

$$J \frac{{\rm d}\omega_{\rm m}}{{\rm d}t} = T_{\rm motor} - T_{\rm load} \tag{12}$$

where subscript '*s*' and '*r*' represents stator and rotor terms, respectively, $p = {\rm d}/{\rm d}t$, J is the moment of inertia and $\omega_{\rm m}$ is the mechanical speed of the motor.

The state-space representation of these (7)–(10) considering a space vector i_s and λ_s as state variables are shown as

$$\frac{{\rm d}i_{\rm s}}{{\rm d}t} = S_1\left(S_2\lambda_{\rm s} - S_3 i_{\rm s} + K_{\rm r}(V_{\rm s} - S i_{\rm s} - {\rm j}\omega_{\rm r}\lambda_{\rm s}) + \frac{{\rm j}\omega_{\rm r} i_{\rm s}}{S_1}\right) \tag{13}$$

$$\frac{{\rm d}\lambda_{\rm s}}{{\rm d}t} = (V_{\rm s} - S i_{\rm s}) \tag{14}$$

where

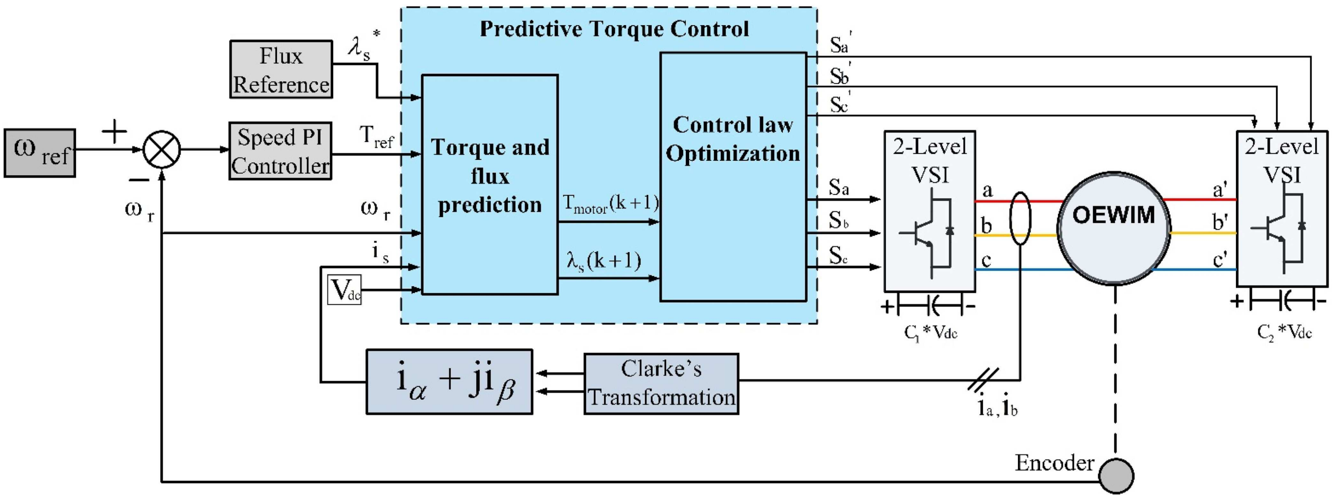

Fig. 2 *Basic PTC block diagram*

$$\left.\begin{array}{l} S = R_s, S_1 = \dfrac{L_m}{L_s L_r - L_m^2}, S_2 = \dfrac{R_r}{L_m}, S_3 = \dfrac{L_s R_r}{L_m} \\ K_r = \dfrac{L_r}{L_m}, i_s = i_{s\alpha} + j i_{s\beta}, \lambda_s = \lambda_{s\alpha} + j\lambda_{s\beta}, \\ V_s = V_{s\alpha} + jV_{s\beta} \end{array}\right\} \tag{15}$$

In PTC algorithm these (13) and (14) are expressed in a discrete manner.

3 Basic PTC

The basic PTC functional block diagram is presented in Fig. 2. Speed PI controller generates torque reference. The input requirements to the PTC algorithm for controlling and realisation of switching states are motor speed, torque reference, flux reference, combined DC-link voltages and measured current. The discretisation of system mathematical model in PTC algorithm uses forward Euler's method. The standard illustration of it is shown as

$$\frac{dx}{dt} = \frac{x(k+1) - x(k)}{T_s} \tag{16}$$

where 'x' is any state variable, 'k' is the present sampling state and 'T_s' is the sample time.

3.1 Measurement and estimation

Direct measurement of machine stator flux is not possible. Due to this, Euler's method is used to estimate the present state stator flux as [42]

$$\lambda_s(k) = \lambda_s(k-1) + T_s((V_s(k-1)) - Si_s(k-1)) \tag{17}$$

The measured currents i_a, i_b and i_c from machine stator terminals undergoes Clarke's transformation, resulting to i_α and i_β terms. From this, current space vector is represented.

3.2 Prediction

The machine current, stator flux and torque are needed to predict for all the accessible switching states. For dual-inverter fed OEWIM, there are 64 (8 × 8) possible switching combinations. Out of these, it offers 37 effective switching combinations. The voltage space-vector representation for VSI-I and VSI-2 are given as (18) and (19). The effective voltage space vector applied to the machine is formulated as (20)

$$V_{s1} = \left(\frac{2}{3}\right)(C_1 \times V_{dc})\left(S_a + S_b e^{j(2\pi/3)} + S_c e^{j(4\pi/3)}\right) \tag{18}$$

$$V_{s2} = \left(\frac{2}{3}\right)(C_2 \times V_{dc})\left(S_{a'} + S_{b'} e^{j(2\pi/3)} + S_{c'} e^{j(4\pi/3)}\right) \tag{19}$$

$$V_s = V_{s1} - V_{s2} \tag{20}$$

Table 1 denotes possible effective inverter switching states and its corresponding phase voltages in a stationary reference frame. For these switching states, space vector locations are presented in Fig. 3. One step ahead predicted flux, current and torque are characterised as [42]

$$\lambda_s(k+1)_n = \lambda_s(k) + T_s((V_s(k))_n - Si_s(k)) \tag{21}$$

$$\begin{aligned} i_s(k+1)_n = i_s(k) + T_s\Bigg(S_1 \Bigg(& S_2\lambda_s(k) - S_3 i_s(k) \\ & + K_r((V_s(k))_n - Si_s(k) - j\omega_r\lambda_s(k)) + \frac{j\omega_r i_s(k)}{S_1}\Bigg)\Bigg) \end{aligned} \tag{22}$$

$$(T_{motor}(k+1))_n = \frac{3}{2}\frac{P}{2}\left(\mathrm{imag}\left(\bar{\lambda}_s(k+1)_n \times i_s(k+1)_n\right)\right) \tag{23}$$

where $n = (V_0, V_1, V_2, \ldots, V_{36})$.

Thus, from (21)–(23), stator flux, current and torque are predicted for one step ahead with the 37 voltage vectors.

3.3 Control law formulation

Basic PTC constitutes single control law [28]. Control law for torque and flux control is shown as

$$G_n = |T^*_{motor} - T_{motor}(k+1)_n| + W|\lambda_s^* - |\lambda_s(k+1)_n|| \tag{24}$$

where T^*_{motor} and λ_s^* are the reference motor torque and flux values, respectively.

This control law value is checked for every possible voltage vector. Among all the possibilities, voltage vector which provides the minimum value of control law is selected as optimal and its corresponding switching states are given to inverter switches. From (24), it can be observed that W (weighting factor) is the only adjustable term. Therefore, optimal voltage vector selection is affected by the relative importance of torque and flux. With the involvement of more number of control parameters, the complexity of weight factor assignment (to provide relative importance to them) increases. This has a direct influence on voltage vector selection. In [26–41], analytical and empirical methods are employed for proper tuning of weight factor which results in complex control.

Table 1 Switching states and voltage vector realisation for dual-inverter fed OEWIM

Space vector (V_s)	VSI-1 (S_a, S_b, S_c)	VSI-2 (S_a', S_b', S_c')	Realisation V_α	V_β
V_0	(0, 0, 0)	(0, 0, 0)	0	0
V_1	(1, 0, 0)	(1, 0, 0)	V_{dc} (0.222)	0
V_2	(1, 1, 0)	(1, 1, 0)	V_{dc} (0.11)	(0.193) V_{dc}
V_3	(0, 1, 0)	(0, 1, 0)	V_{dc} (−0.11)	(0.193) V_{dc}
V_4	(0, 1, 1)	(0, 1, 1)	V_{dc} (−0.222)	0
V_5	(0, 0, 1)	(0, 0, 1)	V_{dc} (−0.11)	(−0.193) V_{dc}
V_6	(1, 0, 1)	(1, 0, 1)	V_{dc} (0.11)	(−0.193) V_{dc}
V_7	(1, 0, 0)	(1, 1, 1)	V_{dc} (0.444)	0
V_8	(1, 0, 0)	(1, 0, 1)	V_{dc} (0.33)	(0.193) V_{dc}
V_9	(1, 1, 0)	(1, 1, 1)	V_{dc} (0.222)	(0.385) V_{dc}
V_{10}	(0, 1, 0)	(0, 1, 1)	0	(0.385) V_{dc}
V_{11}	(0, 1, 0)	(1, 1, 1)	V_{dc} (−0.222)	(0.385) V_{dc}
V_{12}	(0, 1, 0)	(1, 1, 0)	V_{dc} (−0.33)	(0.193) V_{dc}
V_{13}	(0, 1, 1)	(1, 1, 1)	V_{dc} (−0.444)	0
V_{14}	(0, 0, 1)	(1, 0, 1)	V_{dc} (−0.33)	(−0.193) V_{dc}
V_{15}	(0, 0, 1)	(1, 1, 1)	V_{dc} (−0.222)	(−0.385) V_{dc}
V_{16}	(0, 0, 1)	(0, 1, 1)	0	(−0.385) V_{dc}
V_{17}	(1, 0, 1)	(1, 1, 1)	V_{dc} (0.222)	(−0.385) V_{dc}
V_{18}	(1, 0, 0)	(1, 1, 0)	V_{dc} (0.33)	(−0.193) V_{dc}
V_{19}	(1, 0, 0)	(0, 1, 1)	V_{dc} (0.667)	0
V_{20}	(1, 0, 0)	(0, 0, 1)	V_{dc} (0.55)	(0.193) V_{dc}
V_{21}	(1, 1, 0)	(0, 1, 1)	V_{dc} (0.44)	(0.385) V_{dc}
V_{22}	(1, 1, 0)	(0, 0, 1)	V_{dc} (0.33)	(0.577) V_{dc}
V_{23}	(1, 1, 0)	(1, 0, 1)	V_{dc} (0.11)	(0.577) V_{dc}
V_{24}	(0, 1, 0)	(0, 0, 1)	V_{dc} (−0.11)	(0.577) V_{dc}
V_{25}	(0, 1, 0)	(1, 0, 1)	V_{dc} (−0.33)	(0.577) V_{dc}
V_{26}	(0, 1, 0)	(1, 0, 0)	V_{dc} (−0.44)	(0.385) V_{dc}
V_{27}	(0, 1, 1)	(1, 0, 1)	V_{dc} (−0.55)	(0.193) V_{dc}
V_{28}	(0, 1, 1)	(1, 0, 0)	V_{dc} (−0.667)	0
V_{29}	(0, 1, 1)	(1, 1, 0)	V_{dc} (−0.55)	(−0.193) V_{dc}
V_{30}	(0, 0, 1)	(1, 0, 0)	V_{dc} (−0.44)	(−0.385) V_{dc}
V_{31}	(0, 0, 1)	(1, 1, 0)	V_{dc} (−0.33)	(−0.577) V_{dc}
V_{32}	(0, 0, 1)	(0, 1, 0)	V_{dc} (−0.11)	(−0.577) V_{dc}
V_{33}	(1, 0, 1)	(1, 1, 0)	V_{dc} (0.11)	(−0.577) V_{dc}
V_{34}	(1, 0, 1)	(0, 1, 0)	V_{dc} (0.33)	(−0.577) V_{dc}
V_{35}	(1, 0, 1)	(0, 1, 1)	V_{dc} (0.44)	(−0.385) V_{dc}
V_{36}	(1, 0, 0)	(0, 1, 0)	V_{dc} (0.55)	(−0.193) V_{dc}

4 Proposed PTC

It is established that the following are the most prime steps involved in PTC: (i) estimation of unknowns which are not measurable, (ii) system behaviour prediction and (iii) control law minimisation. Due to the key issues faced by basic PTC, this paper proposed a ranking based multi-objective optimisation. It relieves PTC from weighting factor tuning. Fig. 4 depicts the pictorial representation of the proposed control algorithm.

Execution steps for the ranking method are given as follows:

4.1 Step 1: separation of multi objectives

Torque and stator flux are considered as separate objectives (G_1 and G_2). Because of the presence of two VSI bridges (increase in the number of switches), switching frequency is to be limited to minimise overall switching losses in OEWIM drive. This limitation can be easily achieved by considering one more objective (G_3), which reduces state voltage variations. With this, voltage vector

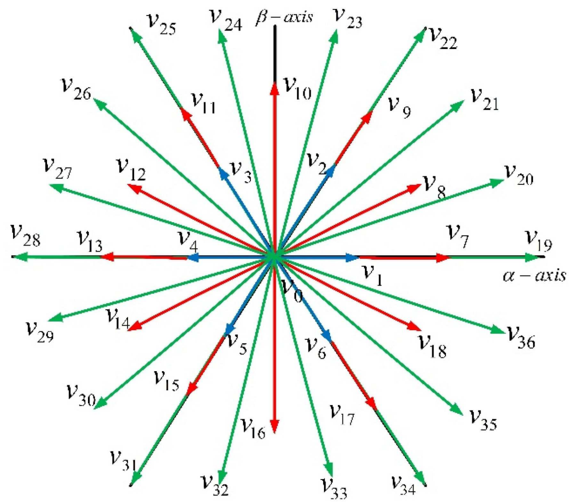

Fig. 3 *Space vector allocations*

remains to be the same for some sample duration and has a direct impact on switching frequency reduction. Therefore multi-objective (G_1, G_2 and G_3) are represented as

$$(G_1)_n = |T^*_{\text{motor}} - T_{\text{motor}}(k+1)_n| \tag{25}$$

$$(G_2)_n = |\lambda^*_s - |\lambda_s(k+1)_n|| \tag{26}$$

$$(G_3)_n = |V_s(k-1) - V_s(k)_n| \tag{27}$$

The above objectives (25)–(27) are formulated with one step ahead. With this, there exist practical sample delay problems which can affect control performance. To circumvent this problem, two-step ahead prediction is preferred. The modified multi-objectives are represented as

$$(G_1)_n = |T^*_{\text{motor}} - T_{\text{motor}}(k+2)_n| \tag{28}$$

$$(G_2)_n = |\lambda^*_s - |\lambda_s(k+2)_n|| \tag{29}$$

$$(G_3)_n = |V_s(k) - V_s(k+1)_n| \tag{30}$$

where

$$(\lambda_s(k+2))_n = \lambda_s(k+1) + T_s((V_s(k+1))_n - Si_s(k+1)) \tag{31}$$

$$i_s(k+2)_n = i_s(k+1) + T_s\left(S_1\left(\begin{matrix} S_2\lambda_s(k+1) - S_3 i_s(k+1) \\ +K_r\left(\begin{matrix}(V_s(k+1))_n - Si_s(k+1) \\ -\mathrm{j}\omega_r\lambda_s(k+1)\end{matrix}\right) \\ +\dfrac{\mathrm{j}\omega_r i_s(k+1)}{S_1}\end{matrix}\right)\right) \tag{32}$$

$$(T_{\text{motor}}(k+2))_n = \frac{3}{2}\frac{P}{2}\left(\text{imag}\left(\bar{\lambda}_s(k+2)_n \times i_s(k+2)_n\right)\right) \tag{33}$$

4.2 Step 2: evaluation and ranking

The multi-objectives (torque (28), flux (29) and switching state variation (30) errors) are evaluated for all the available 37 voltage vectors and rankings (R_1, R_2 and R_3) are assigned corresponding to their values. The value with minimum error assigned lower rank-0 and from this point with increase in error, ranking value also increases.

4.3 Step 3: optimal selection

Each voltage vector constitutes different rankings based on error values of multi-objectives. For a given voltage vector, all the obtained rankings are averaged. The voltage vector (VV) achieving

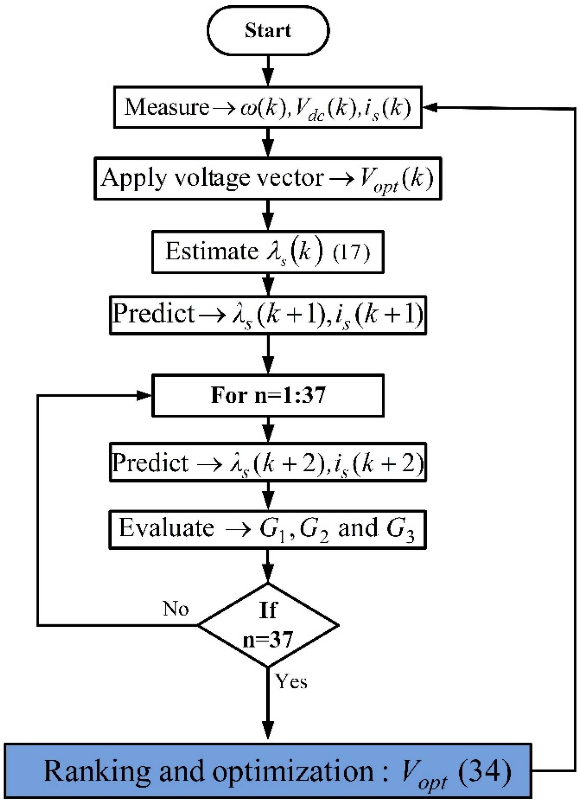

Fig. 4 *Proposed PTC flowchart*

minimum averaged rank value is selected as optimal for the next sampling period. It is represented as

$$V_{\text{opt}} = VV\left[\min\left(\frac{R_1 + R_2 + R_3}{3}\right)\right] \tag{34}$$

The control algorithm is demonstrated for one sampling period. Multi-objective rankings for all the switching states and selection of optimal switching state are represented in Table 2. In this sampling period, voltage vector V_9 offers minimum averaged rank among the all, which is considered as optimal and corresponding switching states are given to dual inverter switches. This control process is completely independent of weighting factor assignment. Thereby, achieving optimal control response for OEWIM drive.

5 Results and discussion

The simulations and real-time experimentation are performed for both conventional and proposed PTC schemes of OEWIM drive. The experimental setup is presented in Fig. 5.

5.1 Simulation results

To validate the proposed control strategy as presented in Section 4, simulation and experimentation are performed on dual-inverter fed OEWIM. Machine modelling is carried out using mathematical (1)–(12) and simulations are executed in Matlab/Simulink environment. The existing machine specifications are presented in Table 3 which are considered for simulation analysis.DC-link voltages of VSI-1 and VSI-2 are set to 333.33 and 166.67 V, respectively, with a combined voltage of 500 V (V_{dc}). The reference value of stator flux is set to 1 Wb (nominal). Both simulation and experiment are run at no load with a sampling time of 100 µs. To study the proposed PTC effectiveness with respect to conventional, conventional weighting factors are designated in basic PTC control law as stated by

$$\begin{aligned} G_n = {} & |T^*_{\text{motor}} - T_{\text{motor}}(k+2)_n| + W_1|\lambda^*_{\text{s}} - |\lambda_{\text{s}}(k+2)_n|| \\ & + W_2|V_{\text{s}}(k) - V_{\text{s}}(k+1)_n| \end{aligned} \tag{35}$$

where W_1 and W_2 are flux and switching frequency weighting factors, respectively.

The flux weighting factor (W_1) selection for conventional PTC is considered from [28, 40], where the ratio of nominal torque and flux value ($T_{\text{nom}}/\lambda_{\text{nom}}$) is considered at starting. Later, this value is adjusted empirically to attain better performance, which is time consuming. Thus, these values are empirically set as $W_1 = 75$ and $W_2 = 0.001$. These are only approximated values.

The results of OEWIM drive are represented in Figs. 6–11. At starting, steady-state behaviour of the machine is analysed. For the reference electrical speed of 250 rad/s, the simulated response of motor speed, current and phase voltage are shown in Figs. 6*a* and *c*. From these simulated results, it is observed that the proposed PTC is exhibiting optimal speed and current response, compared to the basic PTC. For the reference speeds of 100 and 250 rad/s (low and high), the simulated response of motor speed, torque and flux are shown in Figs. 7*a*–*d* top. From these results, optimal torque and flux response are observed in the proposed PTC, exhibiting reduced torque and flux ripples compared to the basic PTC.

To analyse machine dynamics, step changes in reference speed are performed from 150 to 200 rad/s and then 200 to 250 rad/s. The simulated dynamic response of motor speed, torque and flux are shown in Figs. 8*a* and *c*. These results convey forward motoring. The same can be analysed with reverse motoring by feeding reference step changes in the reverse direction, i.e. from −150 to −200 rad/s and then −200 to −250 rad/s. Its simulated motor speed, torque and flux characteristics are shown in Figs. 9*a* and *c*.

Finally, when the motor is operating at 200 rad/s, a step change is triggered from 200 to −200 rad/s which conveys speed reversal. The simulated characteristics (motor speed, torque and flux) are shown in Figs. 10*a* and *c*. From the simulation results, it is observed that the proposed PTC exhibits optimal control performance without making any effort of weighting factor selection.

5.2 Experimental results

For real-time execution, the proposed PTC is tested on 3.7 kW, 1440 RPM OEWIM drive fed by two, two-level VSIs. The interface dSPACE (RTI 1104) setup is used to execute the proposed

Table 2 Control performance in one sample interval

Voltage space vector (V_s)	G_1	G_2	G_3	R_1	R_2	R_3	$\frac{1}{3}\times(R_1+R_2+R_3)$
V_0	2.5908	0.0023	192.4501	18	2	2	7.333333
V_1	1.6611	0.0105	111.1111	13	13	1	9
V_2	1.2221	0.0001	111.1111	10	0	1	3.666667
V_3	2.1517	0.0083	222.2222	16	11	3	10
V_4	3.5205	0.0058	293.9724	23	7	4	11.33333
V_5	3.9595	0.0048	293.9724	25	6	4	11.66667
V_6	3.0299	0.0129	222.2222	20	16	3	13
V_7	0.7315	0.0187	111.1111	6	23	1	10
V_8	0.2924	0.0081	0	2	10	0	4
$\mathbf{V_9}$	**0.1466**	**0.0024**	**111.1111**	**0**	**3**	**1**	**1.333333**
V_{10}	0.783	0.0107	192.4501	7	14	2	7.666667
V_{11}	1.7127	0.0189	293.9724	14	24	4	14
V_{12}	3.0814	0.0164	333.3333	21	21	5	15.66667
V_{13}	4.4501	0.0139	400.6168	28	18	7	17.66667
V_{14}	4.8892	0.0032	384.9002	30	4	6	13.33333
V_{15}	5.3283	0.0075	400.6168	31	9	7	15.66667
V_{16}	4.3986	0.0155	333.3333	27	19	5	17
V_{17}	3.4689	0.0236	293.9724	22	28	4	18
V_{18}	2.1002	0.0211	192.4501	15	25	2	14
V_{19}	0.1982	0.027	192.4501	1	31	2	11.33333
V_{20}	0.6372	0.0164	111.1111	5	20	1	8.666667
V_{21}	1.0763	0.0059	111.1111	8	8	1	5.666667
V_{22}	1.5154	0.0046	192.4501	12	5	2	6.333333
V_{23}	0.5857	0.013	222.2222	4	17	3	8
V_{24}	0.3439	0.0213	293.9724	3	26	4	11
V_{25}	1.2736	0.0295	384.9002	11	34	6	17
V_{26}	2.6423	0.0271	400.6168	19	32	7	19.33333
V_{27}	4.0111	0.0245	444.4444	26	29	8	21
V_{28}	5.3798	0.0219	509.1751	32	27	10	23
V_{29}	5.8188	0.0112	484.3221	34	15	9	19.33333
V_{30}	6.2579	0.0005	484.3221	35	1	9	15
V_{31}	6.697	0.0103	509.1751	36	12	10	19.33333
V_{32}	5.7673	0.0182	444.4444	33	22	8	21
V_{33}	4.8377	0.0262	400.6168	29	30	7	22
V_{34}	3.908	0.0342	384.9002	24	36	6	22
V_{35}	2.5393	0.0317	293.9724	17	35	4	18.66667
V_{36}	1.1705	0.0293	222.2222	9	33	3	15

Bold values represent optimal voltage space vector achieved with the proposed PTC strategy.

algorithm in the discrete platform. The machine parameters are mentioned in Table 3. DC-link voltages are measured using voltage sensors (LV-25). Stator phase currents are measured using two currents sensors (LA-25). From the encoder, motor speed is measured and connected to the dSPACE Incremental Encoder. All these sensed variables are given to control algorithm by ADC BNC connectors. The controlled switching pulses are acquired from dSPACE controller board and interfaced to dual inverter switches using the digital I/O connector.

The steady-state experimental results of motor speed, phase current and voltage for the reference speed 250 rad/s are represented in Figs. 6*b* and *d*. From these, optimal steady-state speed and current characteristics are achieved with the proposed PTC scheme compared to the basic PTC. From the experimental voltage waveforms as shown in Figs. 6*b* and *d*, minimal voltage state transitions are observed in the proposed PTC. The steady-state motor speed, estimated torque and flux response for the reference speeds 100 and 250 rad/s are shown in Figs. 7*a–d* bottom. From these, it is evident that the maximum flux and torque ripple are less in the proposed PTC compared to the basic PTC. For testing dynamic conditions, motor reference speed is varied online from dSPACE control desk software. A step change in reference speed is assigned from 150 to 200 and 200 to 250 rad/s. Its corresponding motor speed, torque and flux response are shown in Figs. 8*b* and *d*. These characteristics signify the forward motoring operation.

For reverse motoring operation, reference speed step changes are considered from −150 to −200 rad/s and −200 to −250 rad/s. The motor speed, torque and flux characteristics are shown in Figs. 9*b* and *d*.

For speed reversal operation, reference speed step changes are considered from 200 to −200 rad/s (forward to reverse motoring). Figs. 10*b* and *d* represent the motor speed, torque and flux dynamic characteristics during speed reversal operation. From the performed dynamic analysis, it is observed that both control schemes provide similar characteristics with reduced steady state ripples. The switching transitions from the available 37 voltage vectors for both basic and proposed PTC at speed 200 rad/s are represented in Figs. 11*a* and *b*. From Fig. 11*b*, minimal switching transitions are observed in the proposed PTC scheme. From the observed experimental results, a comparative tabular structure is prepared as shown in Table 4 to compare maximum torque, flux

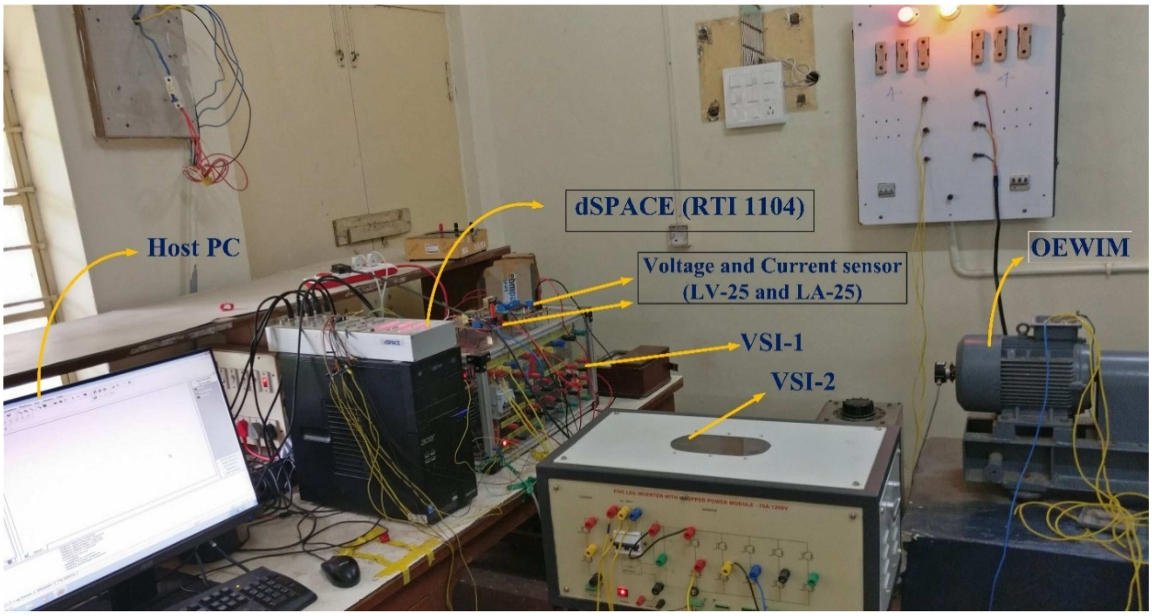

Fig. 5 *Experimental test rig of OEWIM drive*

Table 3 Machine specifications

Parameter	Quantity
stator resistance (R_s)	4.2 Ω
rotor resistance (R_r)	2.6794 Ω
stator inductance (L_s)	0.54 H
rotor inductance (L_r)	0.54 H
mutual inductance (L_m)	0.512 H
poles (P)	4
inertia (J)	0.031 kg/m^2
motor nominal voltage	415 V (line–line)

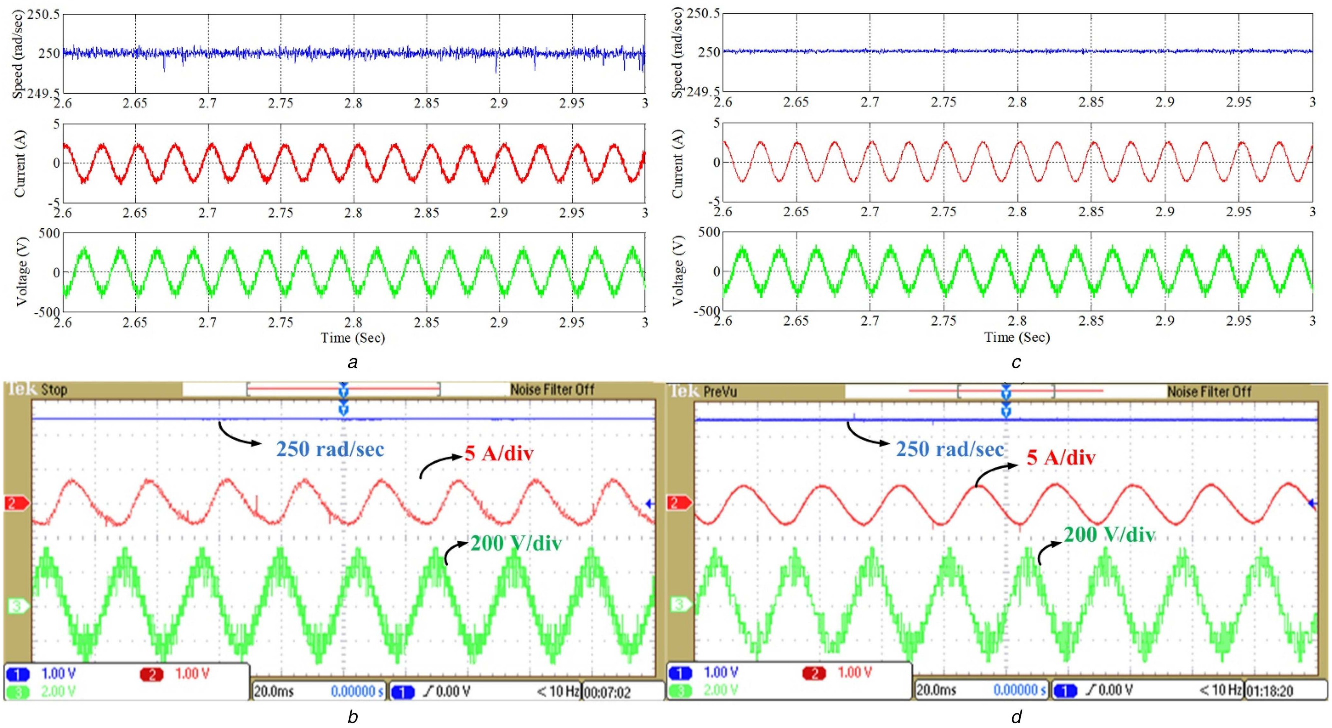

Fig. 6 *Steady-state response of motor speed, current and voltage at 250 rad/s*
(a) Basic PTC simulation, ***(b)*** Basic PTC experimental results, ***(c)*** Proposed PTC simulation, ***(d)*** Proposed PTC experimental results

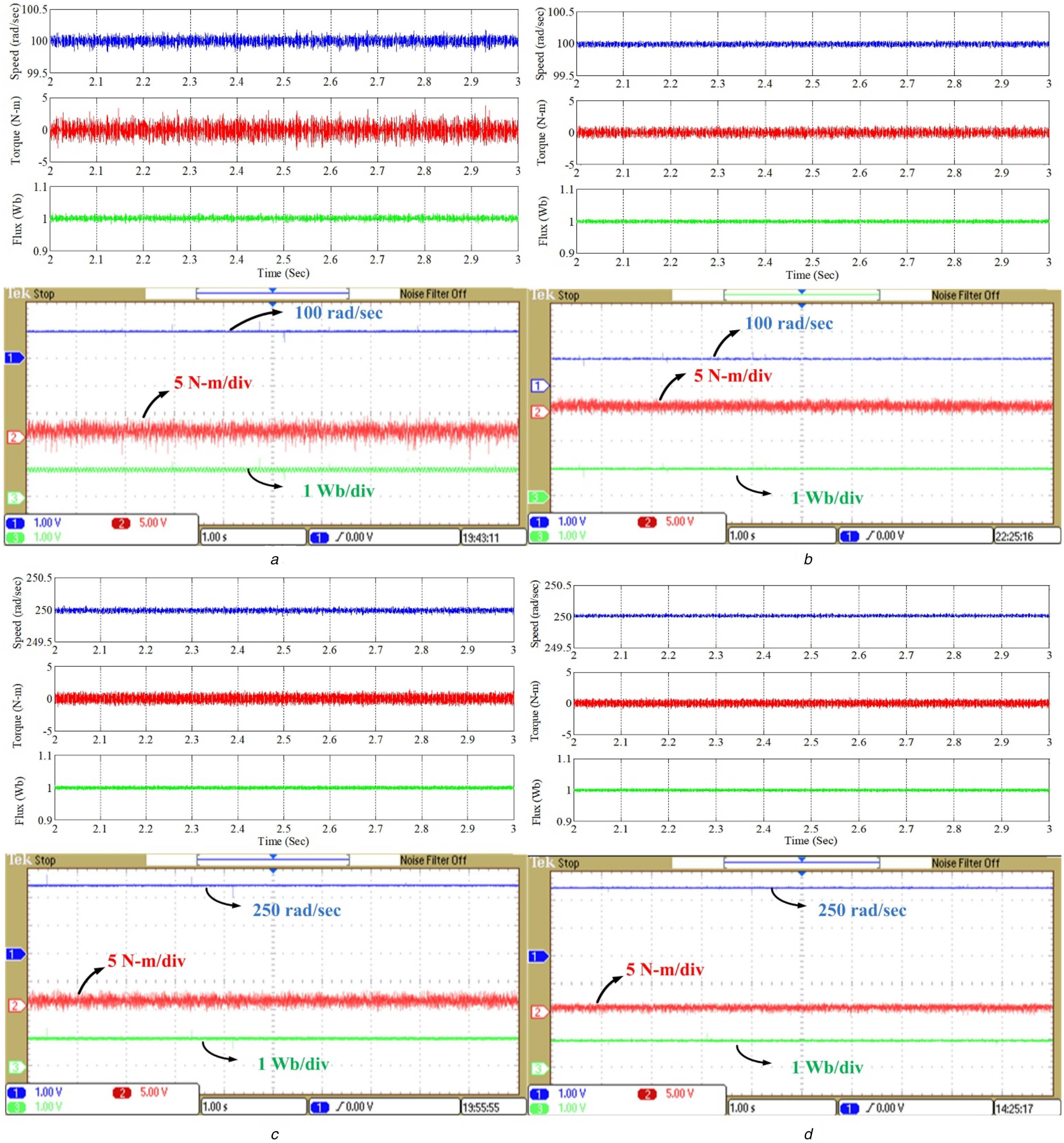

Fig. 7 *Motor speed, torque and flux steady-state characteristics at 100 and 250 rad/s*
(a) Basic PTC simulation and experimental results at 100 rad/s, ***(b)*** Proposed PTC simulation and experimental results at 100 rad/s, ***(c)*** Basic PTC simulation and experimental results at 250 rad/s, ***(d)*** Proposed PTC simulation and experimental results at 250 rad/s

ripples and the average switching frequency of the proposed PTC with the existing control scheme at different operating speeds (100, 150 and 250 rad/s). From these results Figs. 7–11, torque and flux response for the proposed PTC is improved with reduced steady-state ripples compared to the conventional scheme. Switching frequency also minimised compared to a basic control scheme as shown in Fig. 12. This validates optimal control response and effortless control of the proposed PTC over the conventional scheme.

6 Conclusion

In basic PTC, the weighting factor selection in single control law and its tuning determines optimal control response. This is only troublesome and time consuming. This paper proposed a simple ranking method for dual-inverter fed OEWIM drive which relieves PTC from weighting factor assignment. The multiple objectives are considered separately and optimisation is achieved based on minimisation of averaged ranking. The optimised switching states are applied to inverter switches.

To validate the proposed control technique, simulation and experimentation are performed on OEWIM drive considering torque, flux ripple and switching frequency limitation objectives. By considering same control objectives, the proposed PTC is compared with the basic PTC. From the obtained results, it can be observed that the proposed scheme exhibits optimal control by minimising torque, flux ripples and switching frequency without weighting factor assignment. Finally, an improvised and effortless control scheme for optimal control of OEWIM drive is accomplished.

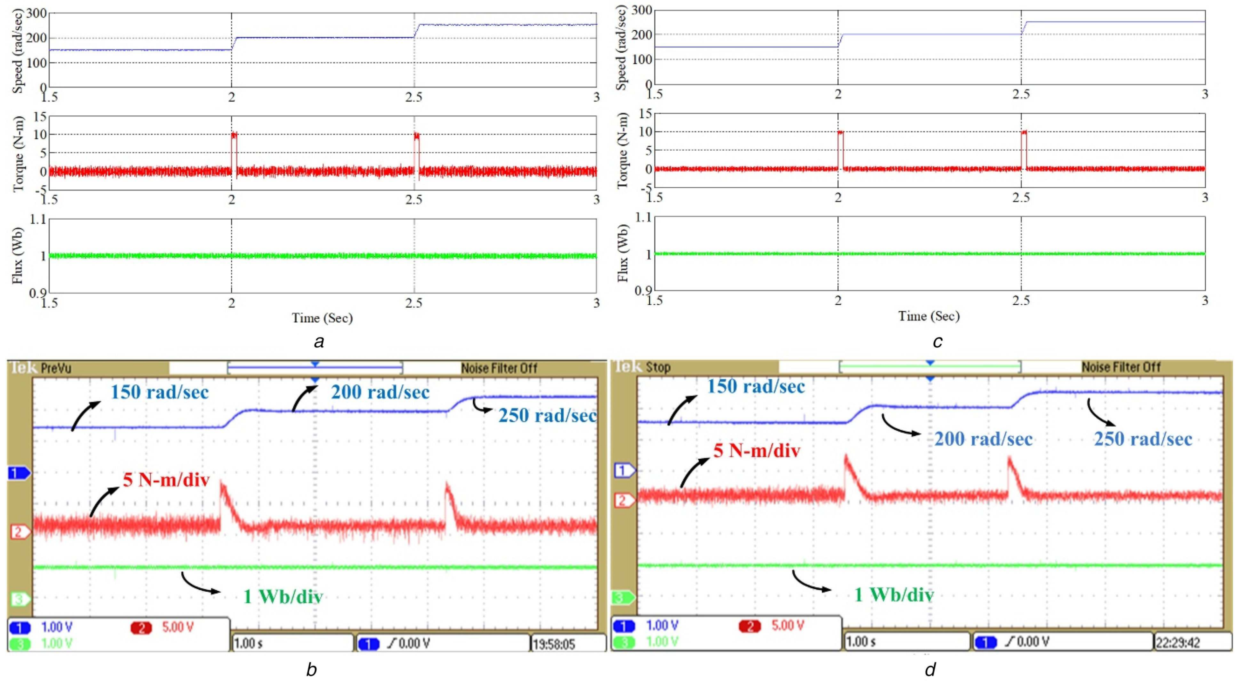

Fig. 8 *Forward motoring speed, torque and flux dynamic characteristics with the step changes in speed from 150 to 200 rad/s and finally 250 rad/s*
(a) Basic PTC simulation, ***(b)*** Basic PTC experimental results, ***(c)*** Proposed PTC simulation, ***(d)*** Proposed PTC experimental results

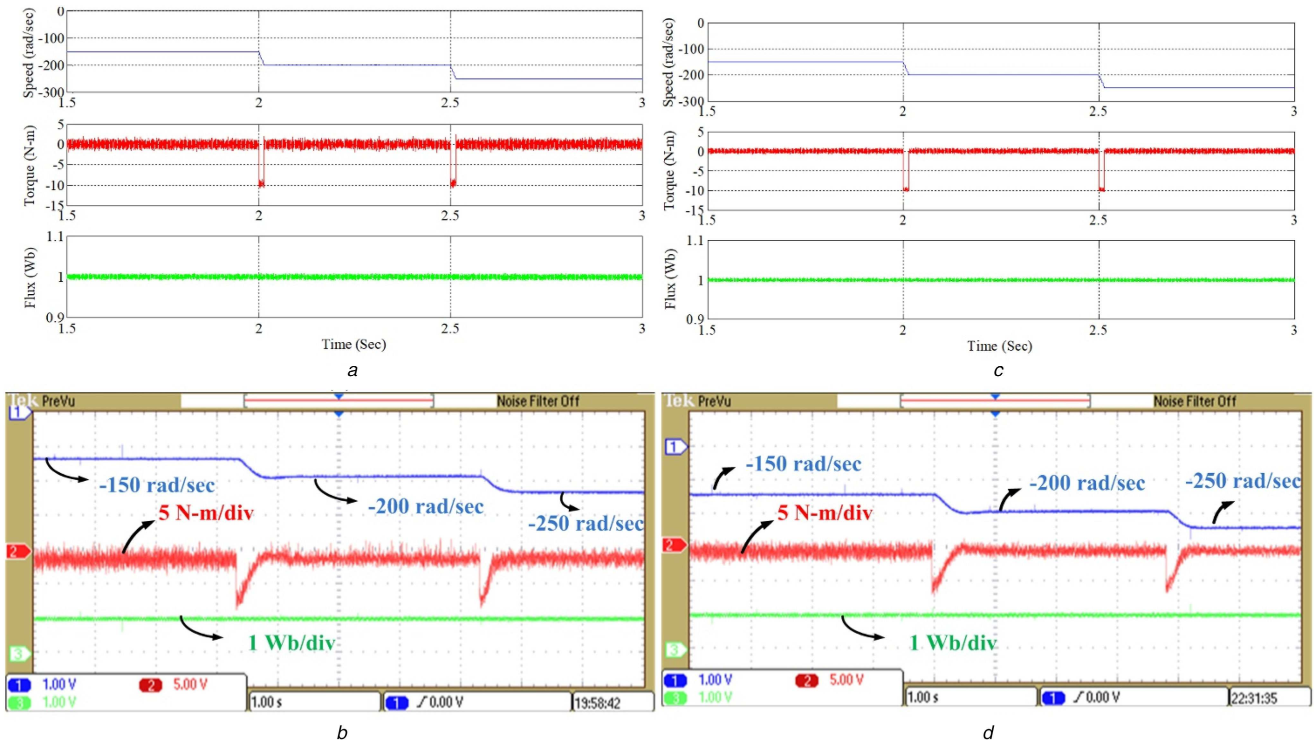

Fig. 9 *Reverse motoring speed, torque and flux dynamic characteristics with the step changes in speed from −150 to −200 rad/s and finally −250 rad/s*
(a) Basic PTC simulation, ***(b)*** Basic PTC experimental results, ***(c)*** Proposed PTC simulation, ***(d)*** Proposed PTC experimental results

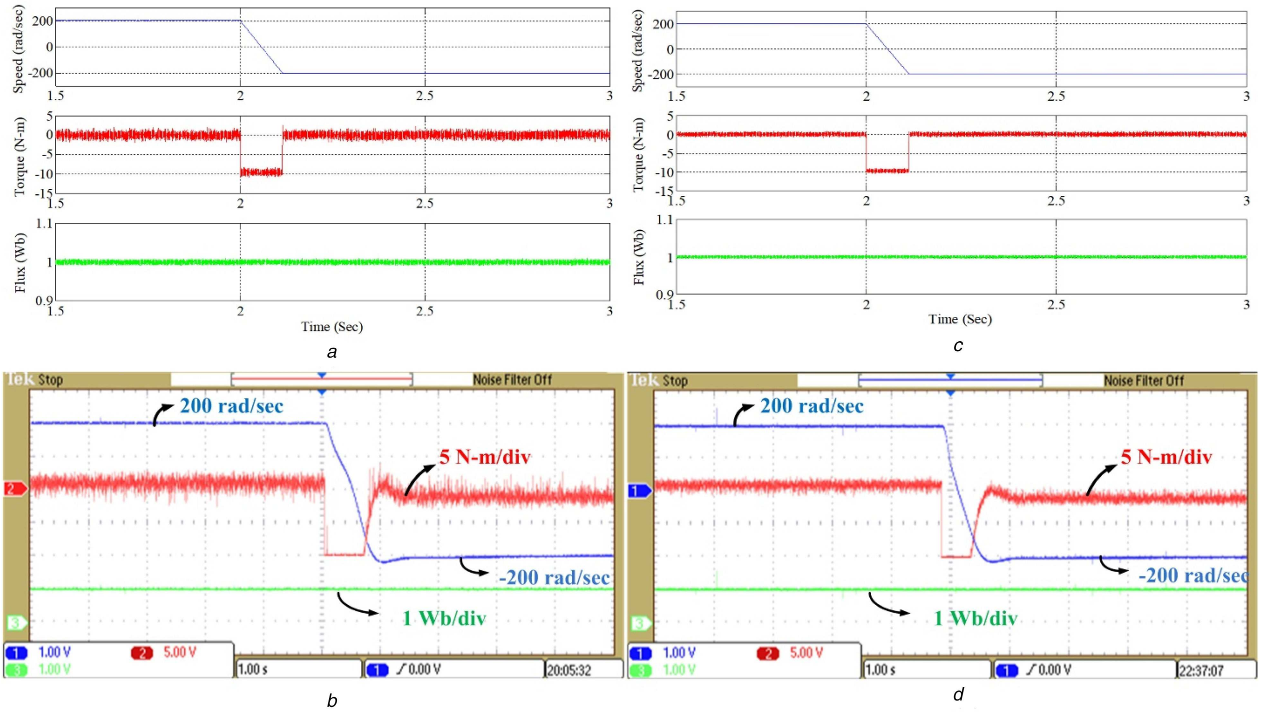

Fig. 10 *Motor speed, torque and flux characteristics during speed reversal operation from +200 to −200 rad/s*
(a) Basic PTC simulation, ***(b)*** Basic PTC experimental results, ***(c)*** Proposed PTC simulation, ***(d)*** Proposed PTC experimental results

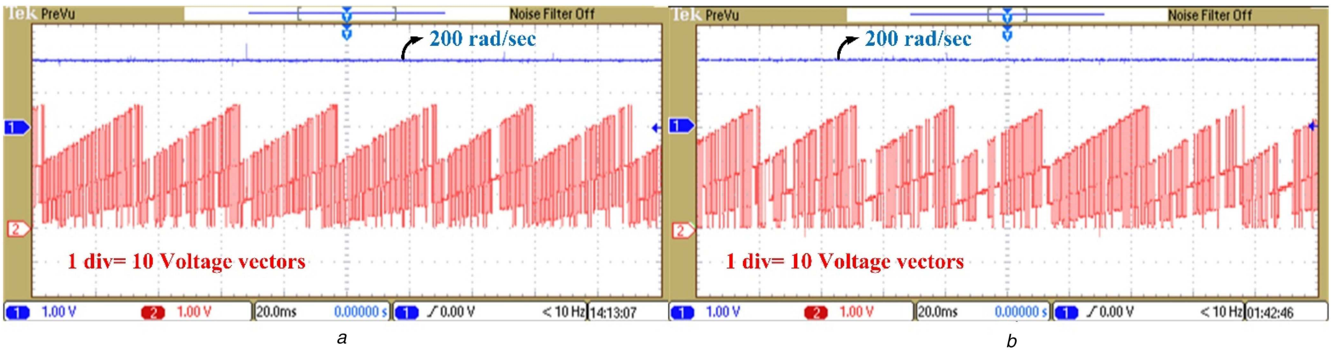

Fig. 11 *Switching transitions at 200 rad/s*
(a) Basic PTC response, ***(b)*** Proposed PTC response

Table 4 Experimental analysis of the proposed PTC with existing scheme

Control scheme	Speed, rad/s	Max. torque ripple, N-m	Max. flux ripple, Wb	Avg. switching frequency, Hz
basic PTC	100	4.5	0.04	3018
proposed PTC		3	0.031	2524
basic PTC	150	4	0.03	3724
proposed PTC		2.8	0.018	3105
basic PTC	250	3	0.02	3458
proposed PTC		1.8	0.012	2965

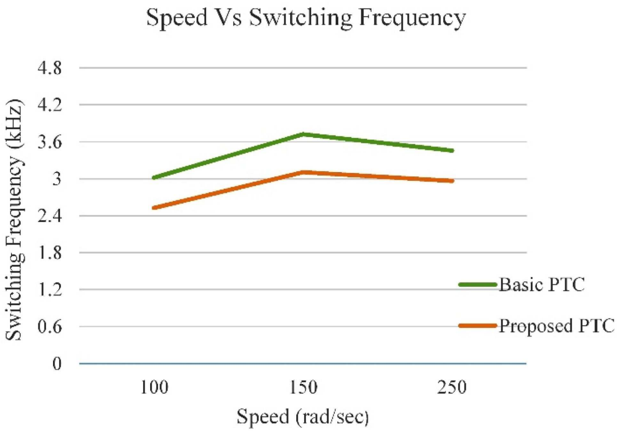

Fig. 12 *Switching frequency comparison at different speeds*

7 References

[1] Kouro, S., Malinowski, M., Gopakumar, K., *et al.*: 'Recent advances and industrial applications of multilevel converters', *IEEE Trans. Ind. Electron.*, 2010, **57**, (8), pp. 2553–2580

[2] Gupta, K.K., Ranjan, A., Bhatnagar, P., *et al.*: 'Multilevel inverter topologies with reduced device count: a review', *IEEE Trans. Power Electron.*, 2016, **31**, (1), pp. 135–151

[3] Mittal, N., Singh, B., Singh, S.P., *et al.*: 'Multilevel inverters: a literature survey on topologies and control strategies'. 2012 2nd Int. Conf. Power, Control and Embedded Systems, Allahabad, 2012, pp. 1–11

[4] Rodriguez, J., Lai, J.S., Peng, F.Z.: 'Multilevel inverters: a survey of topologies, controls, and applications', *IEEE Trans. Ind. Electron.*, 2002, **49**, (4), pp. 724–738

[5] Lakhimsetty, S., Surulivel, N., Somasekhar, V.T.: 'Improvised SVPWM strategies for an enhanced performance for a four-level open-end winding induction motor drive', *IEEE Trans. Ind. Electron.*, 2017, **64**, (4), pp. 2750–2759

[6] Blaschke, F.: 'The principle of field-orientation as applied to the transvector closed-loop control system for rotating-field machines', *Siemens Rev.*, 1972, **34**, pp. 217–220

[7] Kawamura, A., Haft, R.: 'An analysis of induction motor field oriented or vector control'. IEEE Power Electronics Specialists Conf. Rec., 1983, pp. 91–101

[8] Sathikumar, S., Vithayathil, J.: 'Digital simulation of field-oriented control of induction motor', *IEEE Trans. Ind. Electron.*, 1984, **IE-31**, (2), pp. 141–148

[9] Takashi Noguchi, T.: 'A new quick-response and high-efficiency control of an induction motor', *IEEE Trans. Ind. Appl.*, 1986, **22**, (5), pp. 820–827

[10] Kang, J.-K., Sul, S.-K.: 'New direct torque control of induction motor for minimum torque ripple and constant switching frequency', *IEEE Trans. Ind. Appl.*, 1999, **35**, (5), pp. 1076–1082

[11] Lee, K.-B., Song, J.-H., Choy, I., *et al.*: 'Torque ripple reduction in DTC of induction motor driven by three-level inverter with low switching frequency', *IEEE Trans. Power Electron.*, 2002, **11**, pp. 255–264

[12] Kumar, K.V.P., Kumar, T.V.: 'Experimental implementation of direct torque control of open end winding induction motor'. 2016 IEEE Region 10 Conf. (TENCON), Singapore, 2016, pp. 3318–3323

[13] Shyu, K.-K., Lin, J.-K., Pham, V.-T., *et al.*: 'Global minimum torque ripple design for direct torque control of induction motor drives', *IEEE Trans. Ind. Electron.*, 2010, **57**, (9), pp. 3148–3156

[14] Ramchand, R., Gopakumar, K., Patel, C., *et al.*: 'Online computation of hysteresis boundary for constant switching frequency current-error space-vector-based hysteresis controller for VSI fed IM drives', *IEEE Trans. Power Electron.*, 2012, **27**, (3), pp. 1521–1529

[15] Morari, M., Lee, J.H.: 'Model predictive control: past, present and future', *Comput. Chem. Eng.*, 1999, **23**, pp. 667–682

[16] Maciejowski, J.: '*Predictive control with constraints*' (Prentice-Hall, New York, 2002)

[17] Camacho, E., Bordons, C.: '*Model predictive control*' (Springer-Verlag, Berlin, Germany, 2007)

[18] Rawlings, J., Mayne, D.: '*Model predictive control, theory and design*' (Nob Hill Publ., Madison, WI, 2009)

[19] Linder, A., Kennel, R.: 'Model predictive control for electrical drives'. IEEE 36th Power Electronics Specialists Conf., 2005, PESC '05, 2005, pp. 1793–1799

[20] Wang, F., Zhang, Z., Kennel, R., *et al.*: 'Model predictive torque control with an extended prediction horizon for electrical drive systems', *Int. J. Control*, 2015, **88**, (7), pp. 1379–1388

[21] Yaramasu, V., Rivera, M., Narimani, M., *et al.*: 'Finite state model-based predictive current control with two-step horizon for four-leg NPC converters', *J. Power Electron.*, 2014, **14**, (6), pp. 1178–1188

[22] Zhou, D., Zhao, J., Liu, Y.: 'Predictive torque control scheme for three-phase four-switch inverter-fed induction motor drives with DC-link voltages offset suppression', *IEEE Trans. Power Electron.*, 2015, **30**, (6), pp. 3309–3318

[23] Zhou, D., Zhao, J., Li, Y.: 'Model predictive control scheme of five-leg AC-DC-AC converter-fed induction motor drive', *IEEE Trans. Ind. Electron.*, 2016, **63**, (7), pp. 4517–4526

[24] Correa, P., Pacas, M., Rodriguez, J.: 'Predictive torque control for inverter-fed induction machines', *IEEE Trans. Ind. Electron.*, 2007, **54**, (2), pp. 1073–1079

[25] Mutschler, P., Flach, E.: 'Digital implementation of predictive direct control algorithms for induction motors'. Proc. of the IEEE Industry Applications Conf., 1998, pp. 444–451

[26] Cortes, P., Kouro, S., Rocca, B.L., *et al.*: 'Guidelines for weighting factors design in model predictive control of power converters and drives'. Proc. IEEE Int. Conf. Industrial Technology (ICIT'09), 2009, pp. 1–7

[27] Vargas, R., Rodríguez, J., Ammann, U., *et al.*: 'Predictive current control of an induction machine fed by a matrix converter with reactive power control', *IEEE Trans. Ind. Electron.*, 2008, **55**, (12), pp. 4372–4380

[28] Rodríguez, J., Kennel, R.M., Espinoza, J.R., *et al.*: 'High performance control strategies for electrical drives: an experimental assessment', *IEEE Trans. Ind. Electron.*, 2012, **59**, (2), pp. 812–820

[29] Vargas, R., Ammann, U., Hudoffsky, B., *et al.*: 'Predictive torque control of an induction machine fed by a matrix converter with reactive input power control', *IEEE Trans. Power Electron.*, 2010, **25**, (6), pp. 1426–1438

[30] Miranda, H., Cortes, P., Yuz, J., *et al.*: 'Predictive torque control of induction machines based on state-space models', *IEEE Trans. Ind. Electron.*, 2009, **56**, (6), pp. 1916–1924

[31] Habibullah, Md., Lu, D.D.C., Xiao, D., *et al.*: 'A simplified finite-state predictive direct torque control for induction motor drive', *IEEE Trans. Ind. Electron.*, 2016, **63**, (6), pp. 3964–3975

[32] Habibullah, M., Lu, D.D.C.: 'Model predictive duty based torque and flux ripples minimization of induction motor drive'. 7th IET Int. Conf. Power Electronics, Machines and Drives (PEMD 2014), Manchester, 2014, pp. 1–6

[33] Zhang, Y., Yang, H., Xia, B.: 'Model predictive torque control of induction motor drives with reduced torque ripple', *IET Electr. Power Appl.*, 2015, **9**, (9), pp. 595–604

[34] Davari, S.A., Khaburi, D.A., Kennel, R.: 'An improved FCS–MPC algorithm for an induction motor with an imposed optimized weighting factor', *IEEE Trans. Power Electron.*, 2012, **27**, pp. 1540–1551

[35] Zanchetta, P.: 'Heuristic multi-objective optimization for cost function weights selection in finite states model predictive control'. Workshop on Predictive Control of Electrical Drives and Power Electronics, October 2011, pp. 70–75

[36] Muddineni, V.P., Bonala, A.K., Sandepudi, S.R.: 'Enhanced weighting factor selection for predictive torque control of induction motor drive based on VIKOR method', *IET Electr. Power Appl.*, 2016, **10**, (9), pp. 877–888

[37] Muddineni, V.P., Sandepudi, S.R., Bonala, A.K.: 'Finite control set predictive torque control for induction motor drive with simplified weighting factor selection using TOPSIS method', *IET Electr. Power Appl.*, 2017, **11**, (5), pp. 749–760

[38] Zhou, D., Zaho, J., Liu, Y.: 'Online tuning of weighting factors based on Sugeno-fuzzy method in predictive torque control of four-switch three-phase inverter-fed IM'. Int. Symp. Power Electronics, Electrical Drives, Automation and Motion, 2016, pp. 734–739

[39] Zhu, B., Rajashekara, K., Kubo, H.: 'Predictive torque control with zero-sequence current suppression for open-end winding induction machine'. 2015 IEEE Industry Applications Society Annual Meeting, Addison, TX, 2015, pp. 1–7

[40] Kumar, K.V.P., Vinay, T.: 'Predictive torque control of open-end winding induction motor drive fed with multi-level inversion using two two-level inverters', *IET Electr. Power Appl.*, 2018, **12**, (1), pp. 54–62

[41] Uddin, M., Mekhilef, S., Mubin, M., *et al.*: 'Model predictive torque ripple reduction with weighting factor optimization fed by an indirect matrix converter', *Electr. Power Compon. Syst.*, 2014, **42**, (10), pp. 1059–1069

[42] Rodriguez, J., Cortes, P.: 'Predictive control of induction machines', in '*Predictive control of power converters and electrical drives*', vol. **1** (John Wiley & Sons, Ltd.,Chichester, United Kingdom, 2012), pp. 115–132